Ceramics International xxx (xxxx) xxx

Contents lists available at ScienceDirect

Ceramics International

journal homepage: www.elsevier.com/locate/ceramint

A novel co-continuous Si–Zr hybrid phenolic aerogel composite with excellent antioxidant ablation enabled by sea-island-like ceramic structure at high temperature

Huadong Fu, Yan Qin *, Zhengwei Peng, Jipeng Dou, Zhixiong Huang

School of Materials Science and Engineering, Wuhan University of Technology, Wuhan, 430070, PR China

ARTICLE INFO

Handling Editor: Dr P. Vincenzini

Keywords:
Sol-gel processes
Composites
Porosity
Thermal properties
ZrO_2

ABSTRACT

Lightweight phenolic matrix composites are highly potential in ablative thermal protective materials for future aerospace vehicles, and hybrid modification is considered as one of effective ways to improve the oxidation and ablation resistance of phenolic matrix. Herein, the co-continuous silica zirconium hybrid phenolic resin (SZRx) was synthesized, which can be used to prepare lightweight ablation resistant aerogel composites by the sol-gel method. The SZRx aerogel showed stable porous structure and excellent hydrophobicity, and the silicon zirconium hybrid greatly improved the high temperature carbon residue and oxidation resistance of phenolic resin. The SZRx aerogel composites also possessed excellent integrated characteristics of heat protection and insulation, with a linear ablation rate as low as 0.032 mm/s and a back temperature below 200 °C. The synergistic effect of silicon and zirconium formed the multiphase ceramic layer (C, SiO_2, SiC and ZrO_2) with the sea-island-like structure on the surface of the composite material, which can effectively resist high-temperature ablation and aerodynamic exfoliation. This can indicate that silicon zirconium dual element hybrid phenolic resin is the highly competitive matrix for lightweight and ablation resistant composite materials.

1. Introduction

Phenolic resin has important applications in the field of aerospace ablation thermal protection due to its excellent flame retardancy, good processability, high char yield, and low cost [1–3]. The lightweight design of thermal protection materials is one of the effective ways to improve the load and penetration ability of aircraft. For example, the phenolic impregnated carbon ablators (PICA) developed by NASA is the typical lightweight ablative thermal protection material based on phenolic resin, which has been successfully applied in many planetary exploration missions over the past thirty years [4]. In recent years, fiber reinforced phenolic aerogel composites (FPAC) have been widely used in the field of aerospace thermal protection owing to their advantages such as integrated thermal protection and insulation, low density, low cost, etc. [5–7]. However, the antioxidant and ablative properties of phenolic resins are gradually unable to meet the needs of the aerospace thermal protection field under harsh heat flow environments [8,9].

Silicon hybrid modification is considered as the highly promising strategy for improving the antioxidant and ablative properties of phenolic resins [10]. Silicon modified phenolic resin generates residual silica during the ablation process, which forms the liquid phase at high temperatures and serves as the barrier of reactive oxygen species and heat, effectively improving the antioxidant and ablation properties of phenolic resin. Chen et al. used (3-aminopropyl) triethoxysilane as the silicon source to obtain the organic silicon hybrid phenolic resin by one pot method, and prepared the fiber preform reinforced hybrid phenolic aerogel composite. The material showed low density and efficient heat insulation characteristics, and the introduction of organic silicon significantly improved the oxidation resistance and ablation of the phenolic composite [11]. Xiao et al. demonstrated the mechanism of the improvement of antioxidant performance of phenolic compounds silicon hybridization by molecular dynamics simulations. Si atoms belonging to the Si–*O*–Si framework of silicon can be bonded to the molecular structure of PR to inhibit the thermal decomposition of phenolic fragments. The formation of clusters rich in silica is the main reason for the increased antioxidant performance [12].

However, under higher temperature thermal environments (>1800 °C), silicon modified phenolic resin exhibits weak antioxidant ability due to the gradual evaporation of silica. It is reported that introduction transition metal elements such as Ti [13,14], Zr [15,16]

* Corresponding author.
E-mail address: qinyan@whut.edu.cn (Y. Qin).

https://doi.org/10.1016/j.ceramint.2024.03.207
Received 4 January 2024; Received in revised form 8 March 2024; Accepted 15 March 2024
Available online 16 March 2024

into the main or side chains of siloxane can further improve the anti-oxidant and thermal stability of organosilicon. Jiang et al. [17] successfully synthesized zirconium hybrid silicone resin by two-step sol-gel method. The addition of Zr greatly improved the heat resistance of silicone resin. The results of the investigation showed that zirconium hybrid modification showed the potential synergistic effect on the thermal stability of silicone resin. In addition, the introduction of transition metals could promote the catalytic graphitization on pyrolytic carbon (PyC) [18,19], moreover transition metal oxides usually possess higher melting points than silicon, indicating that the co-hybridization modification of phenolic by transition metals and organosilicon may offer positive effect on the application of FPAC in more severe thermal environments.

In this work, a new type of Si–Zr dual element hybrid phenolic resin was prepared by a two-step method. Further, Si–Zr hybrid phenolic resin (SZRx) aerogel composites with the co-continuous structure were obtained by the sol gel process using quartz fiber needle felt (Q_f) as the macro framework. Zirconium propionate was selected as the precursor of Zr in this study, which has relatively high Zr content compared to commonly used zirconium oxychloride and zirconium n-propoxide [17,21], as well as an appropriate hydrolysis rate. The effects of Si/Zr ratio on the microstructure, hydrophobicity, thermal stability and high-temperature oxidation resistance of SZRx aerogels were investigated. Furthermore, we carried out the oxyacetylene flame test on SZRx aerogel composite, and explored the ablation mechanism of potential synergistic effect of silicon zirconium on the phenolic aerogel composite under the harsh environment of high temperature and aerodynamic exfoliation.

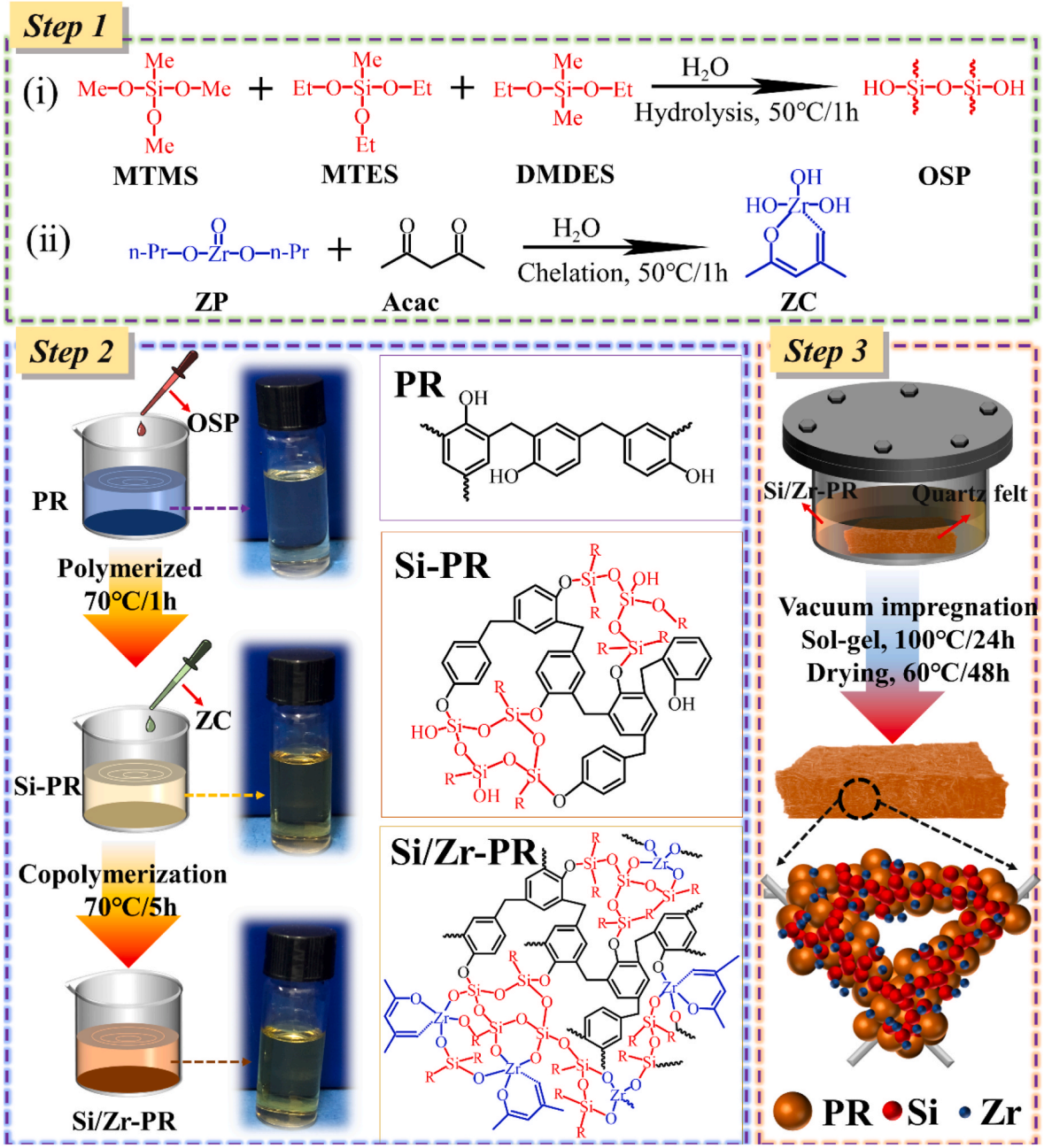

Fig. 1. Synthesis of SZRx and aerogel composites.

2. Experimental

2.1. Materials

The methyl phenolic resin solution (PR, 30w%, isopropanol as solvent) was obtained from Hubei Huahang New Materials Co., Ltd., China. The quartz fiber needle felt with a density of 0.30 g/cm^3 was purchased from Jiangsu Tianniao High tech Co., Ltd. in China. Deionized water was prepared in the laboratory. Methyltrimethoxysilane (MTMS), methyltriethoxysilane (MTES), dimethyldiethoxylsilane (DMDES) and hexamethylenetetramine (HMTA) of analytical grade were purchased from Aladdin Industrial Inc. Zirconium propionate (ZP, $C_6H_{10}O_5Zr$), acetylacetone (Acac) and acetic acid were provided by McLean Inc. All reagents were used without further processing.

2.2. Preparation of silicon-zirconium hybrid phenolic resin (SZRx) and SZRx aerogel composites

SZRx were prepared by two-step method (Fig. 1). Firstly, organic silicon precursor (OSP) and Zirconium chelate (ZC) were synthesized through hydrolysis polymerization (step 1). MTMS, MTES, and DMDES were weighed in a molar ratio of 1:1:1, then poured into a flask and quickly stirred at room temperature for 10 min. Then, according to the molar ratio of acid, water, and alkoxy groups of 0.001:0.8:1, acetic acid and water were evenly mixed, and slowly dropped into the above organic silane mixed solution. The flask was placed in 50 °C water bath and magnetically stirred for 1 h to obtain the solution of the OSP. The ZP, Acac, and water were added to a flask containing isopropanol solution at the molar ratio of 1:1:3. The chelation reaction was carried out in water bath at 50 °C, and the ZC solution was obtained by magnetic stirring for 1h.

According to the formula in Table 1, the OSP solution was added to the phenolic resin solution and magnetically stirred in 70 °C water bath for 1 h to obtain a silicon modified phenolic resin solution (step 2). The ZC solution was further added to the solution and stirred for 5 h to finally obtain a silicon zirconium hybrid phenolic resin solution. Phenolic resins with different Si/Zr ratios were denoted SZRx (x = 0, 1, 2, 3, 4).

Finally, the SZRx aerogel composites were prepared by vacuum impregnation and sol gel process (step 3). The SZRx and HMTA were mixed at the weight ratio of 20:1 and stirred for 60 min to obtain the impregnation solution. The impregnation solution was injected into the metal container containing quartz fiber felt through vacuum induction until the felt was completed filled with resin. The metal container was sealed and placed in an oven at 100 °C, and the sol-gel reacted for 24h. After curing, the composite was taken out and dried in oven at 60 °C under normal pressure for 48h to get SZRx aerogel composite. In addition, SZRx aerogel without fiber reinforcement was also prepared.

2.3. Characterization

Fourier transform infrared spectroscopy (FT-IR, Nexus, US), ^{29}Si nuclear magnetic resonance (NMR, Bruker AVANCEIII 400 M, Germany) and atomic force microscopy (AFM, SPM-9700, Japan) were used to analyze the molecular structure of SZRx. The thermogravimetric analysis (TGA) of the SZRx aerogel in argon atmosphere was performed using the thermogravimetric analyzer (STA449F3, NETZSCH) at the maximum temperature of 1000 °C and heating rate of 10 °C/min. The bulk density of SZRx aerogel composites was measured based on sample volume and weight. The static water contact angle of SZRx aerogel was measured and calculated by the contact angle analyzer (JY-82B, Germany). The high-temperature oxidation resistance of SZRx aerogel was tested by static pyrolysis in muffle furnace at 1000 °C for 20 min. The microstructure and elemental analysis were observed by scanning electron microscopy (SEM-EDS, JSM-7500F, Japan) with energy dispersive spectrometer. The elemental state and phase analysis were conducted using X-ray photoelectron spectroscopy (XPS, ESCALAB 250Xi) and X-ray diffraction (XRD, Empyrean). The degree of graphitization of SZRx aerogel composites was investigated by confocal Raman microscopy (RENISHAW, InVia). The bulk density was measured based on sample volume and weight. The thermal conductivity of samples was tested by the plate method by the thermal constant analyzer (TPS 2500S, Sweden). The ablation performance of the sample was tested by the oxygen acetylene flame system with a flame heat flux density of 2.0 MW/m^2 for 60 s, and the temperature was recorded on the back of the sample using the infrared thermometer. The main parameters of the oxygen acetylene ablation device were shown in Table 2.

Table 1
Formula for SZRx synthesis.

Samples	Phenolic resin solution (g)	Organic silicon precursor (mol)	Zirconium precursor (mol)	Si/Zr ratio
PR	100	0	0	/
SZR0	100	0.5	0	/
SZR1	100	0.475	0.025	19:1
SZR2	100	0.45	0.05	9:1
SZR3	100	0.4	0.1	4:1
SZR4	100	0.25	0.25	1:1

3. Results and discussion

3.1. Molecular structure of SZRx and micro morphology of SZRx aerogel

The organic silicon precursors contain a large amount of Si–OH, which can trigger esterification reaction with PR to obtain the silicon hybrid phenolic resin [20]. Zirconium propionate didn't form zirconia precipitation under the chelation effect of Acac due to the circumvent of severe hydrolysis [21], which allowed the zirconium precursor to present matched hydrolysis rate for copolymerization with the organic silicon precursor and PR. The final synthesized SZRx exhibited the transparent and clear state at macro (Fig. 1). The results of FTIR spectra of PR and SZRx showed that SZRx possessed wide peak of stretching vibration of Si–*O*–Si backbone at 1140 cm^{-1} and 440 cm^{-1} [9,10], as well as the characteristic peak of Si–*O*-Ph at 920 cm^{-1}, compared to PR (Fig. 2a and b) [20]. In addition, the ^{29}Si NMR spectrum also identify either the signal owned to Si–*O*-Ph peak at around −57 ppm (Fig. 2d) [11]. This indicates that OSP underwent self-polymerization reaction to form long chains and some organic silicon were bonded on the molecular chains of phenolic. Meantime, the FTIR spectra of SZR1-SZR4 also showed weak characteristic peaks of Si–*O*–Zr at 610 cm^{-1} [22], implying that some zirconium precursors exist in the SZRx in form of Si–*O*–Zr. Additionally, both of SZR0 and SZR4 exhibited one broad peak near 17.5° corresponding to adjacent chains of the linear polymer [18], indicating that Si and Zr exists as organic covalent bond in SZRx rather than oxidized state (Fig. 2e). The microstructure and elemental distribution of SZR4 in a solvent-free state also confirmed this point. Fig. 2f ~ h showed that no obvious particle structure was found in SZR4 resin at both the micro and nano scales. EDS mapping results showed that the distribution of Zr was relatively uniform, while the distribution of Si was slightly uneven, mainly due to the micro phase separation of organic silicon and phenolic (Fig. 2i).

After curing, the FTIR spectrum of SZRx showed that the stretching vibration peak (-CH_3, C–H on the benzene ring) was significantly

Table 2
Oxygen acetylene ablation parameters.

Heat flux density (MW/m^2)	Torch inner diameter (mm)	Distance (mm)	Gas flow (L/h)		Pressure (MPa)	
			O_2	C_2H_2	O_2	C_2H_2
2.0 ± 02	2	10	714	660	0.4	0.095

Table 3
Thermal stability parameters of PR and SZRx aerogels.

Samples	$T_{10\%}$ (°C)	T_{max} (°C)	$R_{1000°C}$ (%)
PR	270.4	515.7	51.8
SZR0	392.5	547.5	53.9
SZR1	420.5	552.5	54.7
SZR2	441.4	553.9	56.1
SZR3	412.0	553.5	56.9
SZR4	406.7	544.7	58.0

weakened at 2870-3050 cm^{-1} [23], and the C–N stretching vibration peak appeared at 1256 cm^{-1} (Fig. 2c). This indicated that the curing mechanism of SZRx was basically the same as that of PR. The curing agent HMTA was thermally decomposed to produce dimethylhydroxylamine, formaldehyde, and ammonia, which reacted with PR to form cross-linked curing.

To further investigate the state of PR and organosilicon zirconium in SZRx, AFM examination was performed on the cured SZRx (Fig. 3). Based on the phase angle difference of the actual vibration of probe contacting with PR chains and organosilicon (zirconium) chains, the microstructure of the cured brittle sections of PR, SZR0, and SZR4 were obtained, and PR chains presented in the light region and organosilicon (zirconium) chains in the dark region. Compared with pure PR (Fig. 3d), organosilicon hybrid PR (SZR0) showed more obvious light dark boundary at the 1 μm scale, demonstrating that the micro phase separation phenomenon between PR and organosilicon molecular chains in SZR0 (Fig. 3e). This may be ascribed to the difference in solubility parameters between organosilicon and PR, and the phase separation rate is greater than the curing rate. However, the phase diagram of SZR4 showed the relatively uniform phase morphology of light and dark intercross (Fig. 3f), presenting the micro-zone co-continuous structure [9]. This may be ascribed to the copolymerization of zirconium

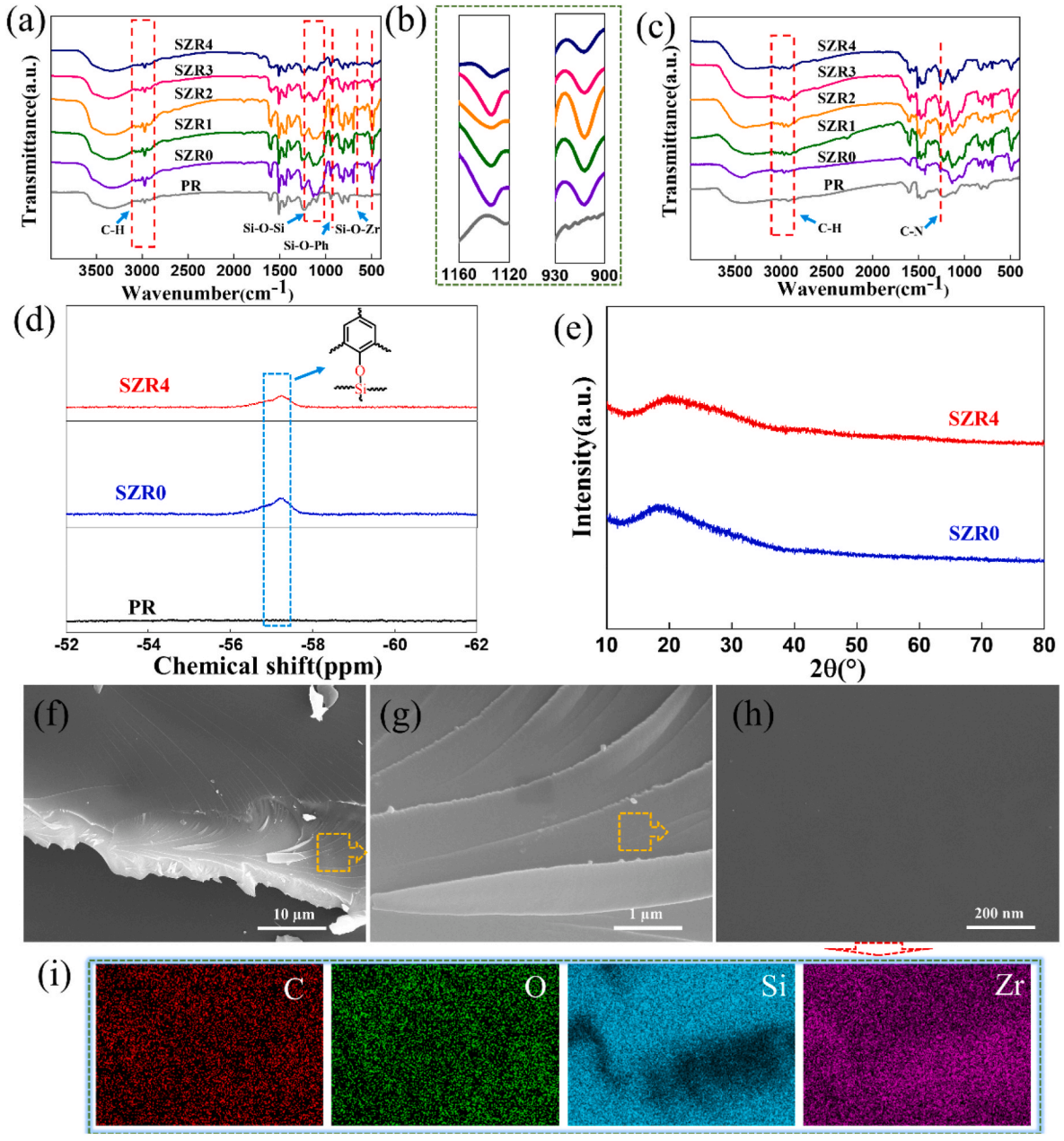

Fig. 2. FTIR spectra of PR and SZRx before (a) (b) and after curing (c). ^{29}Si NMR spectra of PR, SZR0 and SZR4 (d). XRD patterns of SZR0 and SZR4 (e). Microscopic morphology (f ~ h) and EDS mapping results (i) of SZR4 resin in solvent-free state.

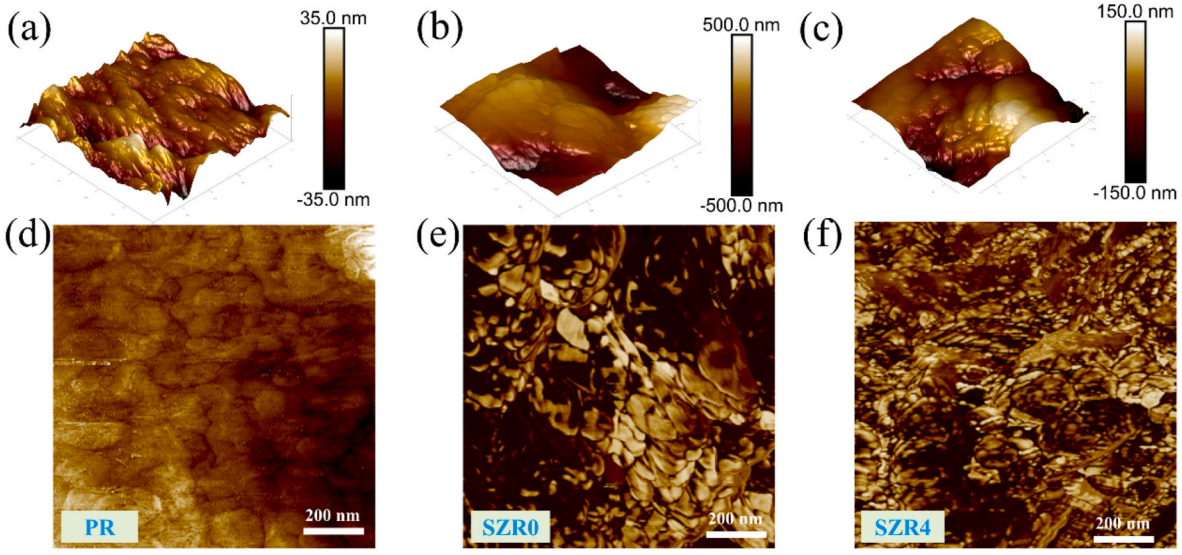

Fig. 3. AFM images. Height image of PR (a), SZR0 (b) and SZR4 (c); Phase image of PR (d), SZR0 (e) and SZR4 (f).

precursor and organosilicon, which improve the compatibility between organosilicon and phenolic aldehyde, and the chelating effect of metal elements with PR make more uniform distribution of zirconium precursor [24].

The micro morphology of the aerogels prepared by PR and SZRx respectively, were showed in Fig. 4a–f. The PR aerogel showed the typical pearl chain-like three-dimensional network porous structure, and the PR particles were uniform in shape, while the silicone hybrid phenolic SZR0 aerogel displayed the coarse skeleton and uneven particle shape, which mainly resulted from the microscopic phase separation of silicone and phenolic during the curing process [25]. With the increased of zirconium relative content, the morphology of SZRx aerogel gradually recovered to similar morphology of pure PR aerogel. Further, the distribution of PR and SZRx aerogel particle size could be analyzed by Image J software. The results showed that the average size of PR aerogel gel particles was 46.5 nm, while SZR0 reached 94.8 nm. The average size

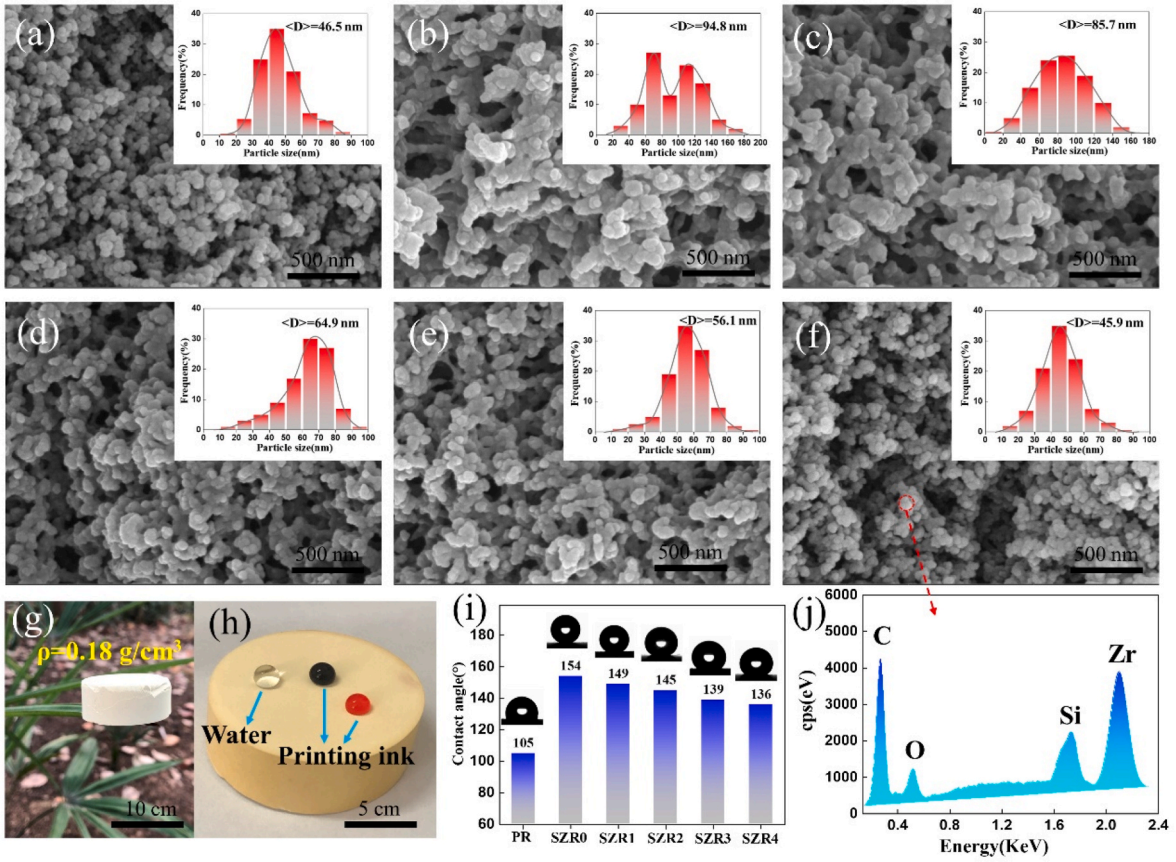

Fig. 4. Aerogel micro morphology and particle size distribution: (a) PR, (b) SZR0, (c) SZR1, (d) SZR2, (e) SZR3, (f) SZR4. (g) SZR4 aerogel on leaves. (f) Liquid on the surface of SZR4 aerogel. (i) Column diagram of PR and SZRx aerogel water contact angle. (j) EDS results on the surface of SZR4 aerogel particles.

of aerogel particles was gradually reduced as the reduction of Si/Zr ratio. Finally, the average size of SZR4 aerogel particles was 45.9 nm, which was almost the same as PR. The energy spectrometer detected that the surface elements of SZR4 aerogel particles were C, O, Si, Zr, and the weight ratio was 70.9:17.5:3.2:8.4 (Fig. 4j), which was close to the feeding ratio of silicon zirconium, indicating that the silicon and zirconium elements were distributed evenly during the formation of SZR4 aerogel particles. It also confirmed that there was no obvious phase separation of silicon zirconium hybrid phenolic resin during the curing process. Therefore, the micro morphology of hybrid resin aerogel can be regulated by the change of Si/Zr ratio, which make the phenolic resin can form the stable aerogel structure and realize the hybrid modification of silicon zirconium elements.

Besides lightweight property (Fig. 4g), SZRx aerogel showed low bulk density of 0.18 g/cm^3 and excellent hydrophobicity, which don't be wetted by pure water and ink (Fig. 4h). As shown in Fig. 4i, the water contact angle of pure PR aerogels was 108°, as the introduction of a large amount of hydrophobic alkyl groups by organic silicon hybridization, the water contact angle of SZR0 aerogels increased to 154°. Although zirconium precursors were added and the water contact angle of aerogels decreased with the reduction of Si/Zr ratio, the water contact angle of SZR4 aerogels still was 136°, which showed good hydrophobicity.

3.2. Thermal stability and antioxidant performance of SZRx aerogel

TGA was used to test the thermal stability of PR and SZRx aerogels, respectively. In argon atmosphere, PR and SZRx aerogels has similar thermogravimetric curves from room temperature to 1000 °C, but the weight loss rate of SZRx aerogels was significantly lower than PR (Fig. 5a). From the data of temperature with 10% weight loss ($T_{10\%}$), residual rate at 1000 °C ($R_{1000°C}$) and maximum thermal decomposition temperature (T_{Max}), SZRx aerogels showed higher residual rate and thermal stability than PR (Table 3). Many studies reported that organic silicon hybridization can improve the thermal stability of phenolic aldehyde [12,20,28,29], and the TGA data of PR and SZR0 also illustrate this point. However, it was worth noting that the thermal stability of silicon zirconium hybrid phenolic aldehyde was better than that of organic silicon hybrid phenolic aldehyde. As the relative content of zirconium increased, the $R_{1000°C}$ of SZRx gradually increased to the maximum of 58.0%, which was 12% and 8% higher than PR and SZR0, respectively, and T_{Max} of SZR1-SZR4 also has improvement (Fig. 5b). This may be ascribed to the inherent drawback of organic silicon hybrid phenolic resin, which organic silicon undergoes the back-bite reaction at high temperatures, produces a large amount of volatile cyclic siloxanes [26,27], and eventually hinders the improvement of thermal stability. In comparison, the chelating effect of zirconium can improve the compatibility between organic silicon and phenolic and the stable zirconium oxide generated by high-temperature pyrolysis may had an inhibitory effect on the formation of cyclic siloxanes. Thus, the silicon zirconium hybridization can further increase the thermal stability of resin.

To further investigated the antioxidant properties of PR and SZRx aerogels respectively, aerogel samples were placed in the muffle furnace at 1000 °C for static pyrolysis for 20 min. The photographs of aerogel samples before and after pyrolysis were shown in Fig. 6a. From the change of aerogel sample size, after high-temperature pyrolysis, PR aerogel experienced more serious volume shrinkage than SZRx aerogels. The weight residue rate of PR aerogel was only 14.2%, while SZRx aerogel exceeded 34%, the highest was 40.6% of SZR2 (Fig. 6b), which demonstrated that the high-temperature oxidation resistance of SZRx aerogel are greatly improved. The microscopic morphology showed that the surface of the residue of PR aerogel was loose and porous after high-temperature pyrolysis (Fig. 6c), and the products of SZR2 and SZR4 aerogel after pyrolysis were relatively hard. Although there were a small number of holes and cracks on the surface owing to the escape and contraction of pyrolysis gas, the surface was generally dense. In addition, the Si/Zr ratio also has impact on the oxidation resistance of hybrid resin aerogel. The SZR2 aerogel with a Si/Zr ratio of 9:1 has the highest weight retention rate. According to the microscopic morphology and energy spectrum analysis, it can be inferred that the surface was covered with the dense silica liquid film (Fig. 6d), which can effectively protect the hybrid resin from the attack of oxygen. However, the hybrid resin SZR4 aerogel with a Si/Zr ratio of 1:1 formed the incomplete liquid film due to the relative reduction of silicon content, and more zirconia particles were presented on the surface (Fig. 6e), which reduced the surface compactness and ultimately lead to the reduction in weight residue rate.

3.3. Ablation resistance and its mechanism of SZRx aerogel composites

Table 4 showed the bulk density and thermal conductivity of PR and SZRx aerogel composites. When the solid content of phenolic resin solution was the same, the silicon zirconium hybrid and silicon zirconium ratio had little effect on the density of aerogel composites, and the bulk density of the five samples was about 0.51 g/cm^3. However, the thermal conductivity of the sample showed a trend of increasing and then decreasing. Silicon hybridization increased the thermal conductivity of aerogel composites, further introduced zirconium, and with the increase of the relative content of zirconium, the thermal conductivity gradually decreased to the initial state. Combined with the above analysis of the micro morphology and pore characteristics of aerogel, the influence of hybridization on the pore size of aerogel led to the change of thermal conductivity.

The oxygen acetylene flame test was the main method for evaluating the ablation performance of composite materials in simulated thermal environments, and its main device was shown in Fig. 7a. Under the flame ablation of 2.0 MW/m^2 heat flux, the thermal response of the sample surface quickly reached to 1900 °C. After 60 s of ablation, the linear ablation rate and weight ablation rate of PR aerogel composites were 0.059 mm/s and 0.015 g/s respectively, while the linear ablation rate of silicon zirconium hybrid phenolic aerogel composites was the lowest of 0.032 mm/s of SZR2, and the weight ablation rate was the lowest of 0.01 g/s of SZR1 (Fig. 7b). The above results indicated that the ablation

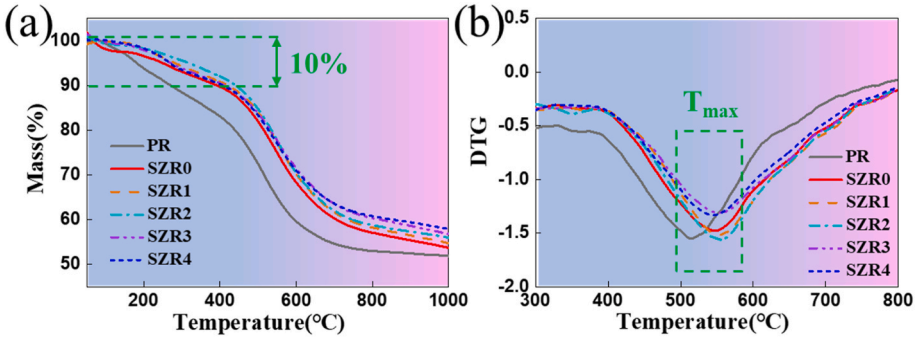

Fig. 5. TG curve (a) and DTG curve (b) of PR and SZRx aerogels.

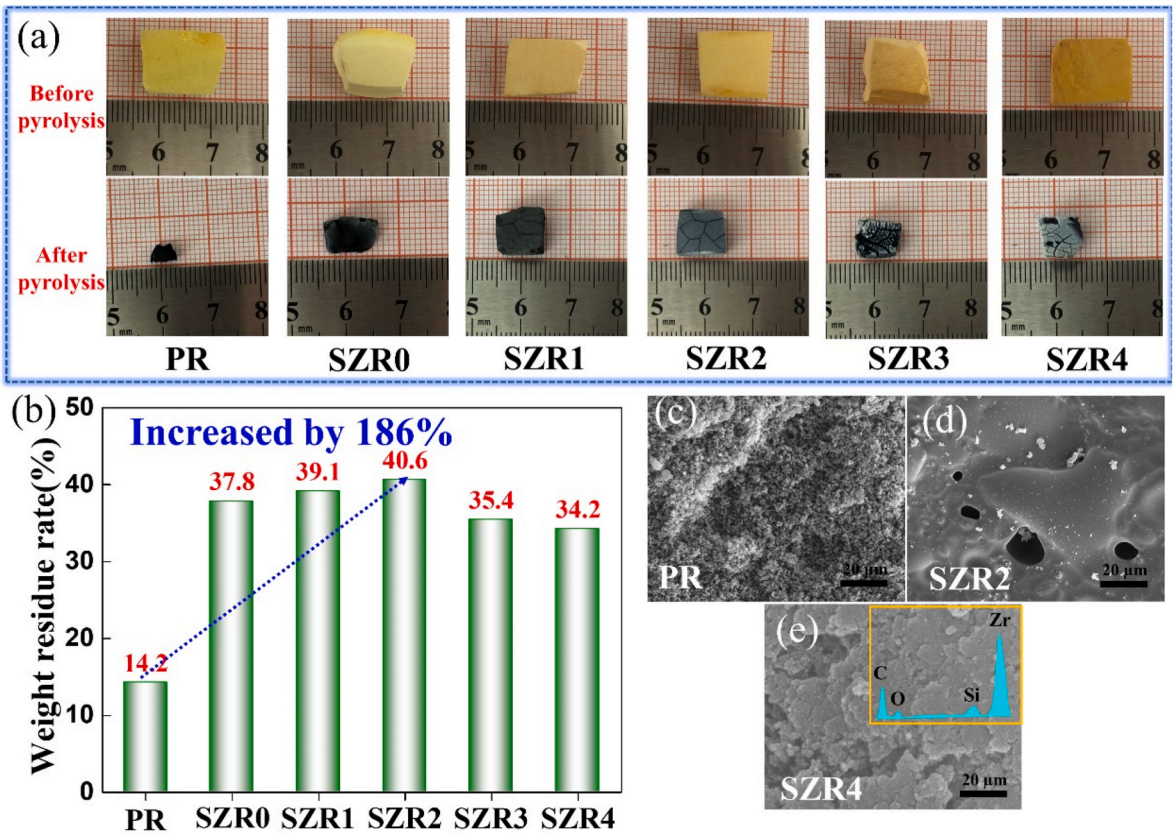

Fig. 6. (a) Photographs before and after static pyrolysis of PR and SZRx aerogels. (b) weight residual rate of PR and SZRx aerogels after static pyrolysis. Micro morphology of PR (c), SZR2 (d) and SZR4 (e) after pyrolysis.

Table 4
Bulk density and thermal conductivity of SZRx aerogel composites.

Samples	PR	SZR0	SZR1	SZR2	SZR3	SZR4
Bulk density (g/cm^3)	0.512	0.508	0.513	0.517	0.505	0.510
Thermal conductivity (W/(m·K))	0.092	0.135	0.129	0.112	0.108	0.102

resistance of phenolic aerogel composites was significantly improved by silicon zirconium hybrid.

The high temperature thermal insulation properties of PR and SZRx aerogel composites were further studied. Fig. 7c showed the cross-section of the samples of PR and SZR2 aerogel composites after ablation. According to the color change, the cross-section could be divided into ablation surface, carbonization and original layer. The improvement of oxidation resistance and ablation resistance of silicon zirconium hybrid made SZR2 aerogel composites have the shallower ablation surface and higher original layer than PR, which meant that SZR2 can retain more complete porous structures at high temperatures, thus blocking heat transfer effectively. Fig. 7d showed the change curve of the central and the back temperature of the ablative surface of PR and SZRx aerogel composites during the ablation process. The central temperature of the ablative surface of the sample kept at about 1900 °C, and the back temperature rise slowly. The back temperature of PR aerogel composites at 60s was 338 °C, while that of SZR2 aerogel composites was lower to 197 °C, showing efficient thermal insulation performance.

Fig. 8 showed the photos and microscopic morphology of the surface of the aerogel composite sample after ablation. In the harsh heat flow environment, the appearance of PR aerogel composite surface formed wrinkles (Fig. 8a), while the surface of SZRx aerogel composite appeared a layer of relatively dense white material after ablation, without obvious wrinkles (Fig. 8e–i, m). The microscopic morphology of the surface of the ablation center showed that the PR aerogel composite presented many pore defects due to the thermal oxidation surface of the matrix, the quartz fiber underwent obvious melting and few PyC particles remained on its surface (Fig. 8b–d). The formation of wrinkles resulted from the enrichment of the melt under the aerodynamic scouring of the surface, which was difficult to produce effective thermal protection for the interior of the composite, and ultimately leaded to the high ablation rate of the composite. Although the surface of the ablation center of SZR0 aerogel composite also showed exposed fibers, there are many carbon residues of matrix pyrolysis. Furthermore, the many fibers didn't undergo melting, and the surface was covered with white matter, which was inferred that the pyrolysis product silicon dioxide attached to the surface of the fiber and PyC (Fig. 8f–h), providing effective thermal protection for the interior of the composite. This also confirms that organosilicon hybrid phenolic resin has good antioxidant and ablation resistance [20,28,29]. However, the ablation center of SZR0 aerogel composite was darker than the surrounding area, which may be ascribed to that the white silicon dioxide in the ablation surface center was blown to the edge by erosion of heat flow, severely weakening the thermal protection effect of the ablation center. The silicon zirconium hybrid phenolic aerogel composite SZR2 presents the dense and uniform white ablative surface and the micro morphology of the ablation center does not show obvious exposed fibers (Fig. 8j-l). Some small holes existed on the surface of SZR2 due to the escape of pyrolysis gas, and some particles are wrapped in the liquid phase. These particles may be composed of zirconia and PyC, and the fiber surface is also wrapped by liquid and particles. The fusion of liquid phase and particles on the ablated surface not only produces effective thermal protection for the interior, but also can resist the erosion of heat flow, which imply that the cooperation of silicon zirconium can greatly improve the ablation and aerodynamic exfoliation resistance of phenolic aerogel composites. With the increasement of the relative content of zirconium, the ablation rate of

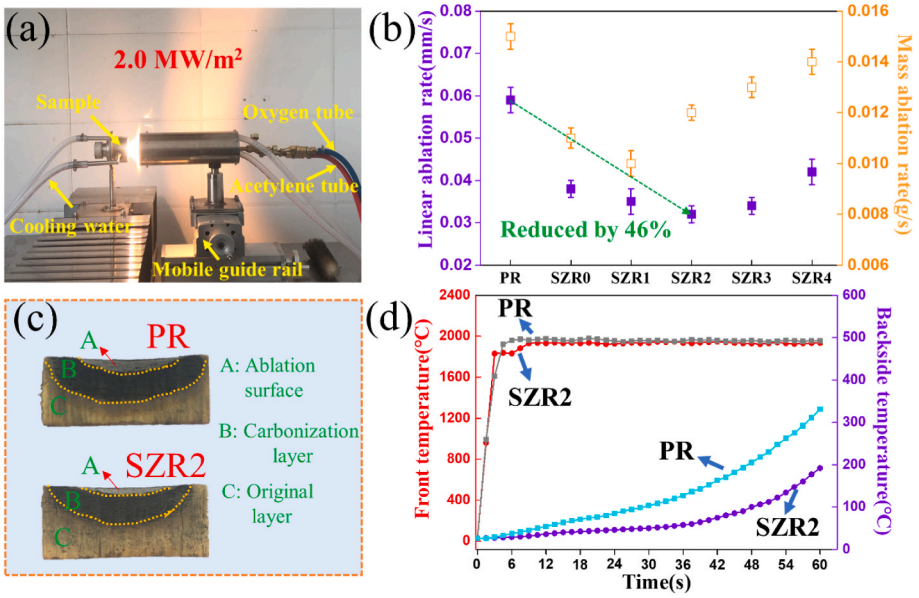

Fig. 7. (a) Oxygen acetylene test device. (b) Linear and mass ablation rates of PR and SZRx aerogel composites. (c) Optical photos of the central section of RP and SZR2 aerogel composites after ablation. (d) The front temperature and back temperature of RP and SZR2 aerogel composites during ablation.

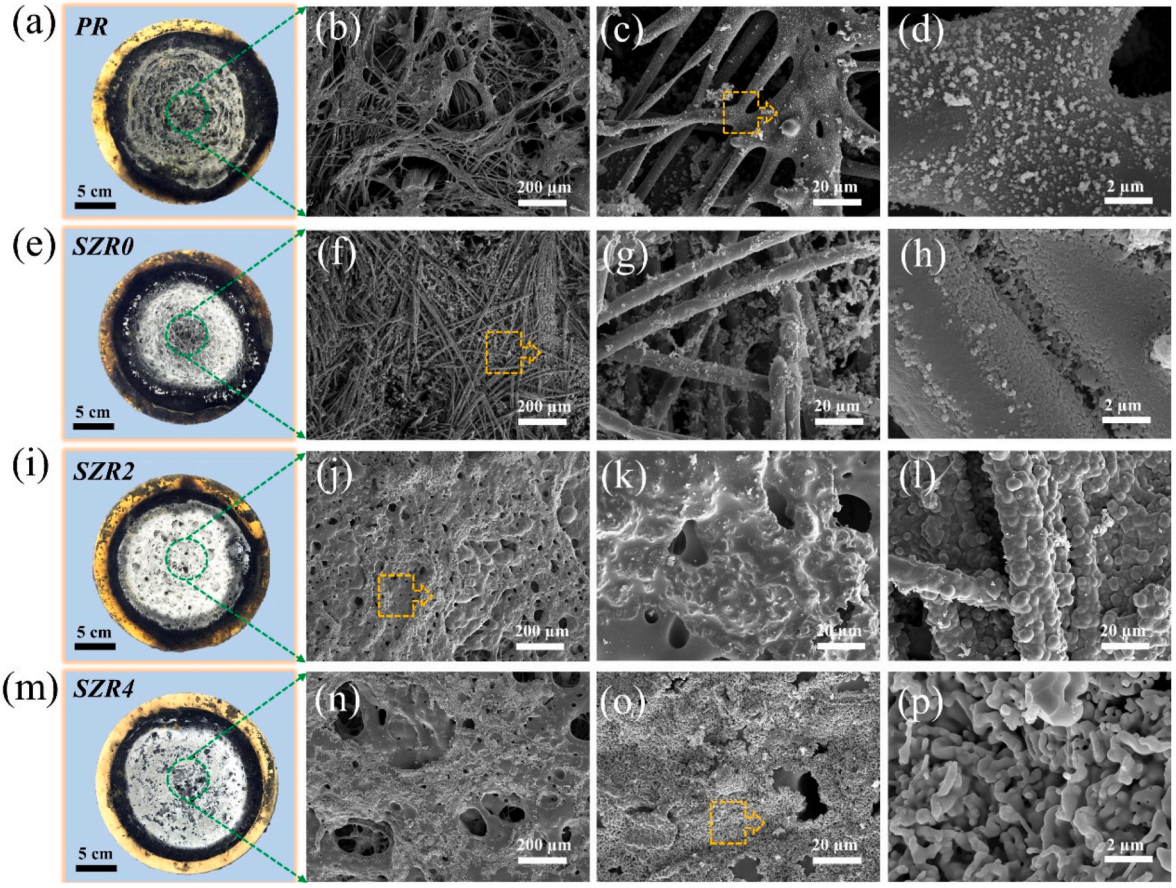

Fig. 8. Surface photos and microscopic morphology of PR aerogel composite (a–d), SZR0 aerogel composites (e–h), SZR2 aerogel composite (i–l) and SZR4 aerogel composites (m–p) after ablation.

SZR4 aerogel composites showed significantly increased. From the microscopic morphology, large holes were observed on the ablation surface, the liquid phase content decreases, and plenty particles gathered to clusters (Fig. 8n-p), further the non-compact clusters formed the channel of heat and oxygen, finally the ablation rate increased.

The phase evolution of PR and SZRx aerogel composites after ablation was studied by XRD and XPS analysis. As shown in Fig. 9b, the ablated surface of PR and SZR0 aerogel composites only showed the

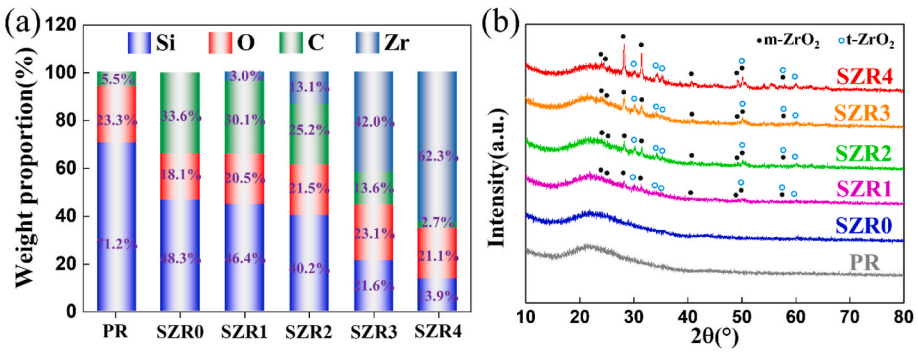

Fig. 9. Surface elements relative content (a), XRD spectrums (b) of PR and SZRx aerogel composites after ablation.

broad peaks at 23–26°which correspond to the superposition of the diffraction peaks of SiO_2 and PyC, among which SiO_2 came from the residual quartz fibers on the surface and the oxidation of the hybrid element Si. Relatively, the ablated surfaces of SZR1∼SZR4 also exhibited characteristic peaks attributed to t-ZrO_2 (PDF#72–1669) and *m*-ZrO_2 (PDF#79–1767), and the intensity of the characteristic peaks increased significantly with the decrease of Si/Zr ratio, indicating that the zirconium element in the hybrid resin exists in the form of zirconia after ablation (Fig. 9b). Furthermore, XPS results showed that the peak of Si 2p gradually weakened at around 103eV, and the peak of Zr 3d [17] gradually strengthened at 185-180eV as the Si/Zr ratio decreased (Fig. 10a and c), which was similar to the changing trend of zirconia peak in XRD (Fig. 9b). From the fitting of Si 2p peak, the silicon element on the SZR2 ablated surface exists in the form of Si–*O*–Si (103.3 eV) [30] and Si–C (101.9 eV) [31] (Fig. 10c and d), indicating that there was still SiC on the ablated surface of the hybrid aerogel composite, which may be caused by the thermal rearrangement of the chains of the silicon hybrid phenolic or the carbothermal reaction of silicon.

In addition, the Si/Zr ratio also affects the degree of graphitization of PyC on the ablated surface of composite materials. R (ID/IG) values of Raman spectroscopy of all samples reflect on the degree of graphitization of PyC. The smaller the R value represent the higher the degree of graphitization of carbon [32]. From the change of R value (Fig. 10b), the hybridization of silicon and zirconium can improve the graphitization degree of pyrolysis carbon and reduce the R value of pyrolysis carbon from the lowest of 2.09 to 1.62, indicating the synergistic catalytic effect of silicon and zirconium on carbon graphitization. The degree of graphitization is proportional to the oxidation resistance of PyC. However, as the Si/Zr ratio further decreased, the pyrolysis carbon R value actually increased, which may be ascribed to the decrease in liquid phase silica and increasement in zirconia, resulting in less graphite carbon dissolved [33].

The relative content change of elements on the ablated surface of the aerogel composite was collected by EDS. As shown in Fig. 9a the relative content of carbon on the ablated surface has significant relationship with the ablation rate. The samples with larger ablation rate usually have less carbon residue on the surface, such as PR and SZR4 aerogel composites, while the samples with higher carbon content, such as SZR2, have lower ablation rate. This is ascribed to that more pyrolysis carbon on the surface can consume more heat through oxidation and reverse radiation, thereby reducing the erosion retreat of the surface [34]. Additionally, the samples with silicon and zirconium content on the surface within moderate range also showed lower ablation rates. The microscopic morphology and energy spectrum analysis showed that

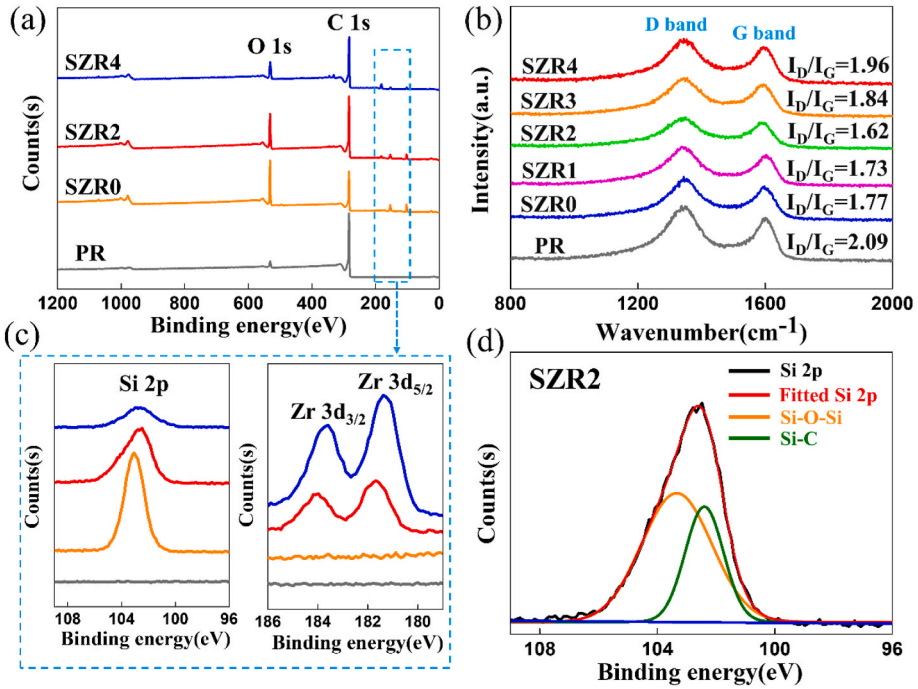

Fig. 10. (a) (c) XPS of ablated surface of RP, SZR0, SZR2 and SZR4 aerogel composites. (b) Raman spectrum of PR and SZRx aerogel composites after ablation. (d) High resolution spectra and fitted peaks of Si in SZR2.

SZR2 aerogel composite possessed the lowest ablation rate (Fig. 11a–c). The liquid phase composed of SiO_2 and SiC evenly wrapped PyC and zirconia particles, which formed dense carbon-containing composite ceramic layer (C, SiO_2, SiC and ZrO_2) with sea-island like structure on the ablation surface, forming the effective barrier for the ablation to expand inward. Meanwhile, the pinning effect of zirconia particles on the surface greatly improves the erosion resistance of the ablation layer.

Interestingly, although the ablation surface of SZR4 aerogel composite also formed the similar structure, the relatively high zirconium content in the matrix caused the enrichment of zirconia particles, and the compactness of the ablation surface reduced due to the lack of liquid phase, which may be the channel for the inward diffusion of heat and oxygen (Fig. 11d–f). More importantly, the carbon ratio on the surface of SZR4 was lower than that of SZR2, indicating that the low silicon zirconium ratio may lead to insufficient oxidation resistance and low carbon residue in the hybrid resin matrix, leading to the increasement of ablation rate.

Based on the above analysis, the mechanism of ablation resistance of PR and SZRx aerogel composites can be demonstrated (Fig. 12). The oxyacetylene flame creates the harsh environment of high temperature, aerodynamic exfoliation, and oxidation on the surface of composite materials. In the process of high temperature ablation of PR aerogel composites, the resin matrix undergoes pyrolysis, carbonization, oxidation, and fiber melting, forming a porous ablation surface. Through the hybridization modification of organic silicon, the oxidation resistance of the matrix was significantly improved, and more PyC was retained on the surface. The liquid phase developed by organic silicon pyrolysis and oxidation forms the relatively dense ablation layer with PyC and fibers, which reduce the ablation rate. However, most of the liquid phase on the ablation center surface was washed to the surrounding area, resulting in obvious exposed fibers on the surface of SZR0 ablation center. The silicon zirconium hybrid phenolic aerogel

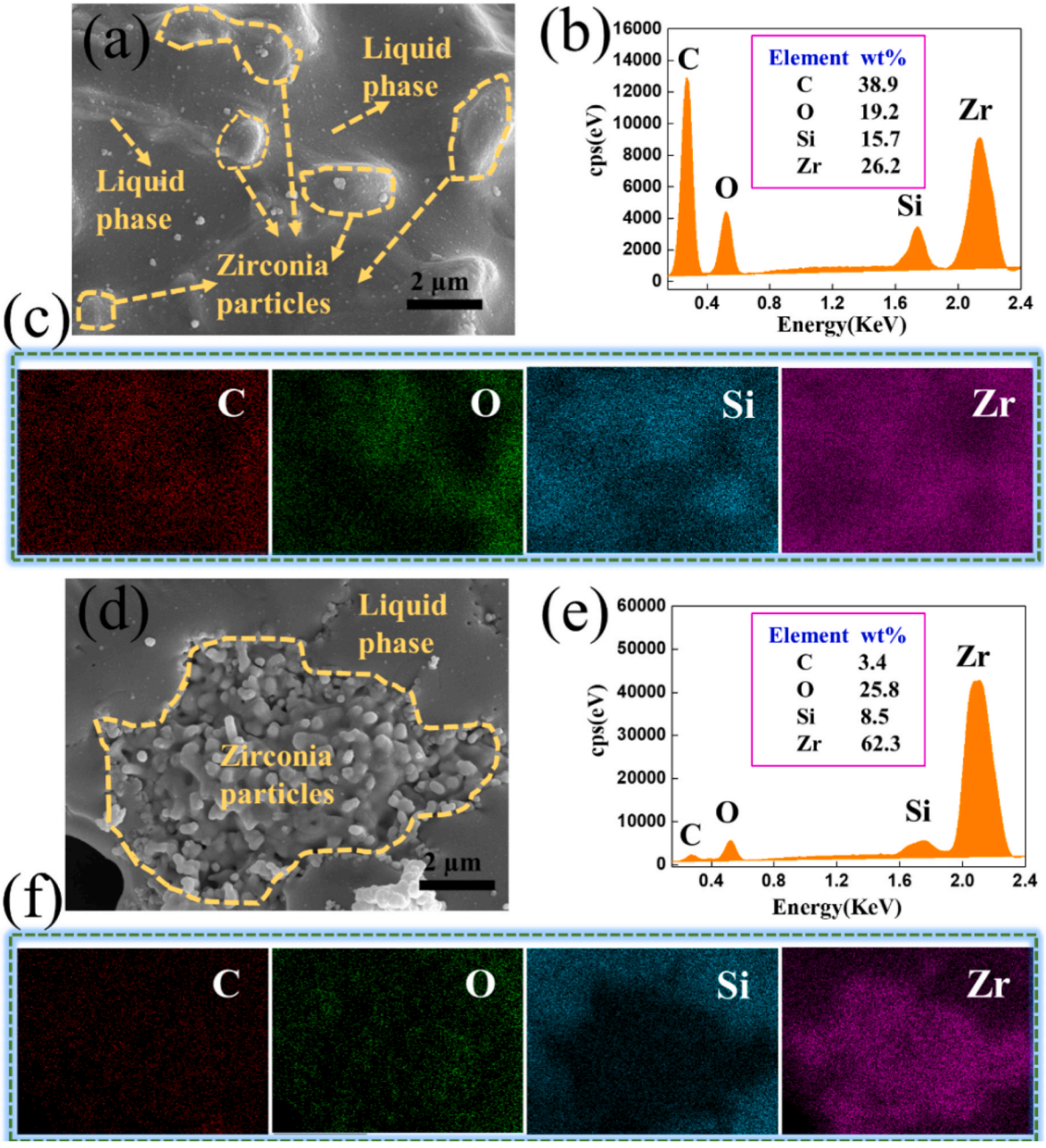

Fig. 11. Surface micro morphology of ablation center of SZR2 aerogel composite (a), EDS results (b), element distribution (c). Surface micro morphology of ablation center of SZR4 aerogel composite (d), EDS results (e), element distribution (f).

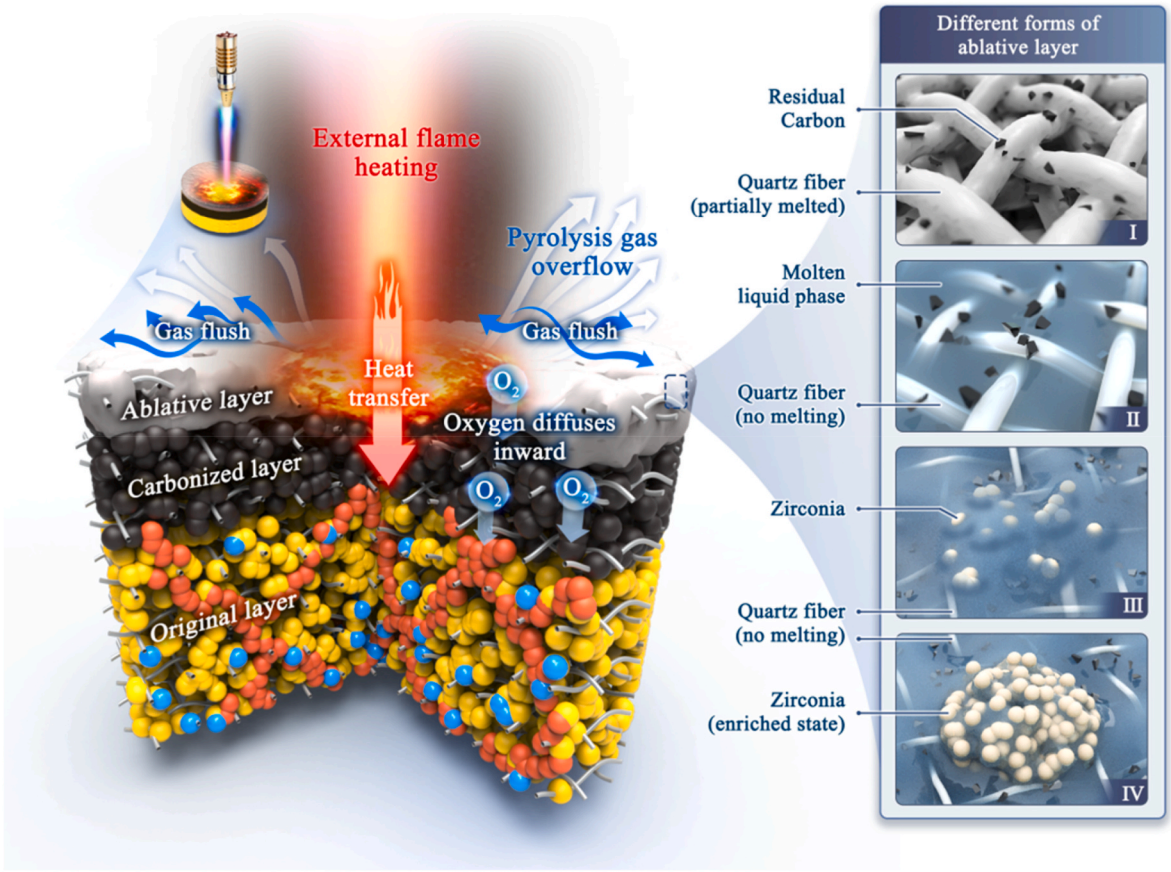

Fig. 12. Ablation mechanism of hybrid resin aerogel composite.

composites were obtained by introducing zirconium element, the chelating effect of zirconium element improves the compatibility of organic silicon and phenolic, and further enhances the oxidation resistance of the matrix and PyC residue. Zirconium was oxidized to zirconia particles with high melting point at high temperature. The liquid phase formed by organic silicon at high temperature wraps PyC and zirconia particles to form the dense multiphase ceramic layer (PyC, SiO_2, SiC and ZrO_2) with sea-island like structure on the ablation surface, which form effective thermal barrier and can resist aerodynamic exfoliation. The synergistic effect of silicon and zirconium significantly improves the ablation resistance of phenolic aerogel. However, when the Si/Zr ratio was low, such as SZR4 aerogel composites with the Si/Zr ratio of 1:1, due to the reduction of the oxidation resistance of the matrix, the content of PyC and liquid phase on the surface was reduced, and the enriched zirconia forms the loose ablation layer, which increases the ablation rate. Therefore, an efficient thermal protection barrier was constructed on the surface of the phenolic aerogel composite with appropriate Si/Zr ratio hybrid.

4. Conclusion

In this work, co-continuous structure SZRx hybrid phenolic resin with adjustable Si/Zr ratio was successfully synthesized by two-step method, and SZRx aerogel composites were prepared by the sol-gel. SZRx aerogel exhibited low density, hydrophobicity, high thermal stability and excellent high-temperature oxidation resistance. The SZRx aerogel composite showed excellent heat resistance and insulation performance, with the linear ablation rate as low as 0.032 mm/s and the back temperature below 200 °C under the heat flow ablation of 2.0 MW/m^2. Moreover , the Si/Zr ratio of 9:1 was set the appropriate ratio to synergistically improve the oxidation resistance and erosion resistance of the composite. At this ratio, more PyC could be retained on the ablated surface of the aerogel composite, and the dense multiphase ceramic layer with sea-island-like structure composed of C, SiO_2, SiC and ZrO_2 can be formed, which can resist high-temperature ablation and aerodynamic exfoliation. The SZRx aerogel composites exhibit excellent integrated characteristics of heat protection and insulation, and have great application potential in the field of light ablative heat protection.

Declaration of competing interest

The authors declare that they have no known competing financial interests or personal relationships that could have appeared to influence the work reported in this paper.

Acknowledgements

This work was founded by the Fundamental Research Funds for the Central Universities (2022-zy-002).

References

[1] M. Natali, J.M. Kenny, L. Torre, Science and technology of polymeric ablative materials for thermal protection systems and propulsion devices: a review, Prog. Mater. Sci. 84 (2016) 192–275, https://doi.org/10.1016/j.pmatsci.2016.08.003.

[2] H.D. Fu, Y. Qin, Z.Y. Zou, J.M. Fan, C.Y. Xue, Enhancement of the interlaminar performance of silica/phenolic laminates after high-temperature pyrolysis using a boron carbide/silicon carbide fibre z-pin, Mater. Des. 219 (2022), https://doi.org/10.1016/j.matdes.2022.110770.

[3] G. Bresson, A. Ahmadi-Senichault, O. Caty, V. Ayvazyan, M.L. Gregori, S.F. Costa, G.L. Vignoles, Thermographic and tomographic methods for tridimensional characterization of thermal transfer in silica/phenolic composites, Compos Part B-Eng 104 (2016) 71–79, https://doi.org/10.1016/j.compositesb.2016.08.022.

[4] Y.W. Pan, X.Y. Jin, H.B. Wang, H. Huang, C. Wu, X.J. Yan, C.Q. Hong, X.H. Zhang, Nano-TiO_2 coated needle carbon fiber reinforced phenolic aerogel composite with low density, excellent heat-insulating and infrared radiation shielding

performance, J. Mater. Sci. Technol. 152 (2023) 181–189, https://doi.org/10.1016/j.jmst.2022.12.035.
[5] Z.L. Yu, N. Yang, V. Apostolopoulou-Kalkavoura, B. Qin, Z.Y. Ma, W.Y. Xing, C. Qiao, L. Bergstrom, M. Antonietti, S.H. Yu, Fire-Retardant and thermally insulating phenolic-silica aerogels, Angew. Chem., Int. Ed. 57 (17) (2018) 4538–4542, https://doi.org/10.1002/anie.201711717.
[6] H.D. Fu, Y. Qin, Z.Y. Zou, J.M. Fan, J.P. Dou, K. Chang, Z.X. Huang, Reinforced compressive and ablative properties of phenolic aerogel by in-situ polycarbosilane-derived ceramic, Ceram. Int. 49 (24) (2023) 40392–40402, https://doi.org/10.1016/j.ceramint.2023.09.365.
[7] B. Niu, H.Y. Zhang, Z. Qian, H.C. Shen, Z. Jiang, X.F. Zhang, Y. Cao, Y.Y. Zhang, D. H. Long, Micro-fracture behaviors of needled short-chopped fiber reinforced phenolic aerogel composites based on in-situ X-ray micro-CT, Compos. Commun. 33 (2022), https://doi.org/10.1016/j.coco.2022.101224.
[8] P.J. Xu, X.L. Jing, High carbon yield thermoset resin based on phenolic resin, hyperbranched polyborate, and paraformaldehyde, Polym. Adv. Technol. 22 (12) (2011) 2592–2595, https://doi.org/10.1002/pat.1806.
[9] Q. Yuan, Y. Wang, Y.S. Huang, J.F. Tian, Z.G. Heng, M. Liang, Y. Chen, H.W. Zou, Nano Co-continuous structure poly(imide-siloxane)/phenolic hybrid resin fabricated by copolymerization for the thermal protection system, Ind. Eng. Chem. Res. 62 (27) (2023) 10477–10486, https://doi.org/10.1021/acs.iecr.3c00969.
[10] R.Y. Yin, H.M. Cheng, C.Q. Hong, X.H. Zhang, Synthesis and characterization of novel phenolic resin/silicone hybrid aerogel composites with enhanced thermal, mechanical and ablative properties, Compos Part a-Appl S 101 (2017) 500–510, https://doi.org/10.1016/j.compositesa.2017.07.012.
[11] H.M. Cheng, Z.H. Fan, C.Q. Hong, X.H. Zhang, Lightweight multiscale hybrid carbon-quartz fiber fabric reinforced phenolic-silica aerogel nanocomposite for high temperature thermal protection, Compos Part a-Appl S 143 (2021), https://doi.org/10.1016/j.compositesa.2021.106313.
[12] J. Xiao, H.Q. Zhang, X. Gao, H.Y. Wang, G.D. Fang, B. Wang, C.Q. Hong, S. H. Meng, Insight into pyrolysis behavior of silicone-phenolic hybrid aerogel through thermal kinetic analysis and ReaxFF MD simulations, Chem. Eng. J. 458 (2023), https://doi.org/10.1016/j.cej.2023.141480.
[13] J.J. Chen, Z. Fu, H.C. Huang, Z.H. Chen, X.R. Zeng, A facile route to prepare homogeneous silicone resin doped with titanium, J. Appl. Polym. Sci. 136 (32) (2019), https://doi.org/10.1002/app.47834.
[14] H.P. Xiang, J.F. Ge, S.H. Cheng, H.M. Han, S.W. Cui, Synthesis and characterization of titania/MQ silicone resin hybrid nanocomposite via sol-gel process, J. Sol. Gel Sci. Technol. 59 (3) (2011) 635–639, https://doi.org/10.1007/s10971-011-2538-0.
[15] J.Y. Bae, S. Yang, J.H. Jin, K. Jung, J.S. Kim, B.S. Bae, Fabrication of transparent methacrylate zirconium siloxane hybrid materials using sol-gel synthesized oligosiloxane resin, J. Sol. Gel Sci. Technol. 58 (1) (2011) 114–120, https://doi.org/10.1007/s10971-010-2363-x.
[16] N.A. Belov, A.N. Tarasenkov, N.A. Tebeneva, N.G. Vasilenko, G.A. Shandryuk, Y. P. Yampolskii, A.M. Muzafarov, Synthesis and gas-transport properties of iron-and zirconium-containing polydimethylsiloxanes, Polym. Sci. B 60 (3) (2018) 405–413, https://doi.org/10.1134/S1560090418030016.
[17] J. Jiang, X.Y. Yuan, K.L. Xue, M. Liu, Y.D. Huang, L. Liu, Novel hybrid zirconium-silicone resin as high-temperature adhesive and an insight into the thermal resistance mechanism, Chem. Eng. J. 446 (2022), https://doi.org/10.1016/j.cej.2022.137350.
[18] S.J. Ko, G.H. Lee, Y.C. Shin, W.I. Lee, S.H. Yum, H. Kim, Improvement of ablation resistance of epoxy composites reinforced with low concentrations of multi walled carbon nanotubes, Compos Part a-Appl S 124 (2019), https://doi.org/10.1016/j.compositesa.2019.105471.
[19] N. Yang, K. Lu, Effects of transition metals on the evolution of polymer-derived SiOC ceramics, Carbon 171 (2021) 88–95, https://doi.org/10.1016/j.carbon.2020.08.072.
[20] Q. Wu, J. Jiang, F. Xie, C. Cui, Z. Hua, L. Liu, Y. Huang, Novel hybrid silicone resin composites with excellent low dielectric and high temperature mechanical properties, Compos. Commun. 35 (2022), https://doi.org/10.1016/j.coco.2022.101288.
[21] C.Q. Liu, K.Z. Li, H.J. Li, S.Y. Zhang, Y.L. Zhang, The effect of zirconium incorporation on the thermal stability and carbonized product of phenol-formaldehyde resin, Polym. Degrad. Stabil. 102 (2014) 180–185, https://doi.org/10.1016/j.polymdegradstab.2014.01.013.
[22] C.Q. Liu, L.Y. Zhang, X. Li, X.J. Chang, Y.T. Wu, X.F. Wang, Synthesis, characterization, and ceramization of a carbon-rich SiC_w-ZrC-ZrB_2 preceramic polymer precursor, Ceram. Int. 45 (13) (2019) 16097–16104, https://doi.org/10.1016/j.ceramint.2019.05.126.
[23] Y. Wang, S.J. Wang, C. Bian, Y.H. Zhong, X.L. Jing, Effect of chemical structure and cross-link density on the heat resistance of phenolic resin, Polym. Degrad. Stabil. 111 (2015) 239–246, https://doi.org/10.1016/j.polymdegradstab.2014.11.016.
[24] X.S. Wu, Y.Z. Zhu, B.B. Pei, P. Cai, Z.R. Huang, Effect of $FeCl_2$ on the pore structure of porous carbon obtained from phenol formaldehyde resin and ethylene glycol, Mater. Lett. 215 (2018) 50–52, https://doi.org/10.1016/j.matlet.2017.12.049.
[25] W.J. Yuan, F.H. Chen, S. Li, Y.P. Du, Z.H. Luo, Y.A. Sun, H. Li, T. Zhao, Synthesis of silicon hybrid phenolic resins with high Si-content and nanoscale phase separation structure, Processes 8 (9) (2020), https://doi.org/10.3390/pr8091129.
[26] S.B. Wang, X.X. Yang, Z.S. Li, X. Xu, H. Liu, D. Wang, H.H. Min, S.B. Shang, Novel eco-friendly maleopimaric acid based polysiloxane flame retardant and application in rigid polyurethane foam, Compos. Sci. Technol. 198 (2020), https://doi.org/10.1016/j.compscitech.2020.108272.
[27] Q. Yuan, L.W. Yan, J.F. Tian, S. Xia, Z.G. Heng, M. Liang, Y. Chen, H.W. Zou, Poly (dimethyl-diphenyl-imide)siloxane/phenolic-based double network hybrid resin coatings for ablation thermal protection, Prog. Org. Coating 182 (2023), https://doi.org/10.1016/j.porgcoat.2023.107693.
[28] Y.P. Du, Z.H. Luo, Y. Yang, Y.M. Yang, W.J. Yuan, H. Li, Y.Q. Hong, Z. Dai, P. X. Zhang, T. Zhao, Theoretical and experimental investigations into the pyrolysis mechanisms of silicon-modified phenolic resin under high temperatures, Carbon 201 (2023) 504–519, https://doi.org/10.1016/j.carbon.2022.07.061.
[29] C. Li, Z.Z. Ma, X.W. Zhang, H. Fan, J.T. Wan, Silicone-modified phenolic resin: relationships between molecular structure and curing behavior, Thermochim. Acta 639 (2016) 53–65, https://doi.org/10.1016/j.tca.2016.07.011.
[30] X.Y. Jin, C. Liu, H. Huang, R.Q. Pan, C. Wu, X.J. Yan, H.B. Wang, Y.W. Pan, C. Q. Hong, X.H. Zhang, Multiscale, elastic, and low-density carbon fibre/siliconoxycarbide-phenolic interpenetrating aerogel nanocomposite for ablative thermal protection, Compos Part B-Eng 245 (2022), https://doi.org/10.1016/j.compositesb.2022.110212.
[31] A. Avila, I. Montero, L. Galan, J.M. Ripalda, R. Levy, Behavior of oxygen doped SiC thin films: an x-ray photoelectron spectroscopy study, J. Appl. Phys. 89 (1) (2001) 212–216, https://doi.org/10.1063/1.1332796.
[32] Z. Wang, T.T. Yan, L.Y. Shi, D.S. Zhang, In situ expanding pores of dodecahedron-like carbon frameworks derived from MOFs for enhanced capacitive deionization, Acs Appl Mater Inter 9 (17) (2017) 15068–15078, https://doi.org/10.1021/acsami.7b02712.
[33] Z.B. Lei, Y. Xiao, L.Q. Dang, W.S. You, G.S. Hu, J. Zhang, Nickel-catalyzed fabrication of SiO_2, TiO_2/graphitized carbon, and the resultant graphitized carbon with periodically macroporous structure, Chem. Mater. 19 (3) (2007) 477–484, https://doi.org/10.1021/cm061806m.
[34] J. Xiao, O. Das, R.A. Mensah, L. Jiang, Q. Xu, F. Berto, Ablation behavior studies of charring materials with different thickness and heat flux intensity, Case Stud. Therm. Eng. 23 (2021), https://doi.org/10.1016/j.csite.2020.100814.